

T2K measurements of muon neutrino and antineutrino disappearance using 3.13×10^{21} protons on target

K. Abe,⁵³ N. Akhlaq,⁴⁴ R. Akutsu,⁵⁴ A. Ali,³¹ C. Alt,¹⁰ C. Andreopoulos,^{51,33} M. Antonova,¹⁸ S. Aoki,³⁰ T. Arihara,⁵⁶ Y. Asada,⁶⁵ Y. Ashida,³¹ E.T. Atkin,²⁰ Y. Awataguchi,⁵⁶ G.J. Barker,⁶² G. Barr,⁴¹ D. Barrow,⁴¹ M. Batkiewicz-Kwasniak,¹⁴ A. Beloshapkin,²⁵ F. Bench,³³ V. Berardi,²¹ L. Berns,⁵⁵ S. Bhadra,⁶⁶ S. Bolognesi,⁵ T. Bonus,⁶⁴ B. Bourguille,¹⁷ S.B. Boyd,⁶² A. Bravar,¹² D. Bravo Berguño,¹ C. Bronner,⁵³ S. Bron,¹² A. Bubak,⁴⁹ M. Buizza Avanzini,⁹ S. Cao,¹⁵ S.L. Cartwright,⁴⁸ M.G. Catanesi,²¹ A. Cervera,¹⁸ D. Cherdack,¹⁶ G. Christodoulou,¹¹ M. Cicerchia,^{23,*} J. Coleman,³³ G. Collazuol,²³ L. Cook,^{41,27} D. Coplowe,⁴¹ A. Cudd,⁶ G. De Rosa,²² T. Dealtry,³² C.C. Delogu,²³ S.R. Dennis,³³ C. Densham,⁵¹ F. Di Lodovico,²⁹ S. Dolan,¹¹ T.A. Doyle,³² J. Dumarchez,⁵⁰ P. Dunne,²⁰ A. Eguchi,⁵² L. Eklund,¹³ S. Emery-Schrenk,⁵ A. Ereditato,² A.J. Finch,³² G.A. Fiorentini,⁶⁶ C. Francois,² M. Friend,^{15,†} Y. Fujii,^{15,†} R. Fukuda,⁵⁷ Y. Fukuda,³⁶ K. Fusshoeller,¹⁰ C. Giganti,⁵⁰ M. Gonin,⁹ A. Gorin,²⁵ M. Guigue,⁵⁰ D.R. Hadley,⁶² P. Hamacher-Baumann,⁴⁷ M. Hartz,^{59,27} T. Hasegawa,^{15,†} S. Hassani,⁵ N.C. Hastings,¹⁵ Y. Hayato,^{53,27} A. Hiramoto,³¹ M. Hogan,⁷ J. Holeczek,⁴⁹ N.T. Hong Van,^{19,26} T. Honjo,⁴⁰ F. Iacob,²³ A.K. Ichikawa,³¹ M. Ikeda,⁵³ T. Ishida,^{15,†} M. Ishitsuka,⁵⁷ K. Iwamoto,⁵² A. Izmaylov,²⁵ N. Izumi,⁵⁷ M. Jakkapu,¹⁵ B. Jamieson,⁶³ S.J. Jenkins,⁴⁸ C. Jesús-Valls,¹⁷ P. Jonsson,²⁰ X. Junjie,⁵⁴ P.B. Jurj,²⁰ M. Kabirnezhad,⁴¹ H. Kakuno,⁵⁶ J. Kameda,⁵³ S.P. Kasetti,³⁴ Y. Kataoka,⁵³ Y. Katayama,⁶⁵ T. Katori,²⁹ E. Kearns,^{3,27,‡} M. Khabibullin,²⁵ A. Khotjantsev,²⁵ T. Kikawa,³¹ H. Kikutani,⁵² S. King,²⁹ J. Kisiel,⁴⁹ T. Kobata,⁴⁰ T. Kobayashi,^{15,†} L. Koch,⁴¹ A. Konaka,⁵⁹ L.L. Kormos,³² Y. Koshio,^{39,‡} A. Kostin,²⁵ K. Kowalik,³⁷ Y. Kudenko,^{25,§} S. Kuribayashi,³¹ R. Kurjata,⁶¹ T. Kutter,³⁴ M. Kuze,⁵⁵ L. Labarga,¹ J. Lagoda,³⁷ M. Lamoureux,²³ D. Last,⁴² M. Lawe,³² R.P. Litchfield,¹³ S.L. Liu,³⁸ A. Longhin,²³ L. Ludovici,²⁴ X. Lu,⁴¹ T. Lux,¹⁷ L.N. Machado,²² L. Magaletti,²¹ K. Mahn,³⁵ M. Malek,⁴⁸ S. Manly,⁴⁵ L. Maret,¹² A.D. Marino,⁶ L. Marti-Magro,^{53,27} T. Maruyama,^{15,†} T. Matsubara,¹⁵ K. Matsushita,⁵² C. Mauger,⁴² K. Mavrokoridis,³³ E. Mazzucato,⁵ N. McCauley,³³ J. McElwee,⁴⁸ K.S. McFarland,⁴⁵ C. McGrew,³⁸ A. Mefodiev,²⁵ M. Mezzetto,²³ A. Minamino,⁶⁵ O. Mineev,²⁵ S. Mine,⁴ M. Miura,^{53,‡} L. Molina Bueno,¹⁰ S. Moriyama,^{53,‡} Th.A. Mueller,⁹ L. Munteanu,⁵ Y. Nagai,⁶ T. Nakadaira,^{15,†} M. Nakahata,^{53,27} Y. Nakajima,⁵³ A. Nakamura,³⁹ K. Nakamura,^{27,15,†} Y. Nakano,³⁰ S. Nakayama,^{53,27} T. Nakaya,^{31,27} K. Nakayoshi,^{15,†} C.E.R. Naseby,²⁰ T.V. Ngoc,^{19,¶} V.Q. Nguyen,⁵⁰ K. Niewczas,⁶⁴ Y. Nishimura,²⁸ E. Noah,¹² T.S. Nonnenmacher,²⁰ F. Nova,⁵¹ J. Nowak,³² J.C. Nugent,¹³ H.M. O’Keeffe,³² L. O’Sullivan,⁴⁸ T. Odagawa,³¹ T. Ogawa,¹⁵ R. Okada,³⁹ K. Okumura,^{54,27} T. Okusawa,⁴⁰ R.A. Owen,⁴⁴ Y. Oyama,^{15,†} V. Palladino,²² V. Paolone,⁴³ M. Pari,²³ W.C. Parker,⁴⁶ S. Parsa,¹² J. Pasternak,²⁰ M. Pavin,⁵⁹ D. Payne,³³ G.C. Penn,³³ L. Pickering,³⁵ C. Pidcott,⁴⁸ G. Pintaudi,⁶⁵ C. Pistillo,² B. Popov,^{50,**} K. Porwit,⁴⁹ M. Posiadala-Zezula,⁶⁰ A. Pritchard,³³ B. Quilain,⁹ T. Radermacher,⁴⁷ E. Radicioni,²¹ B. Radics,¹⁰ P.N. Ratoff,³² C. Riccio,³⁸ E. Rondio,³⁷ S. Roth,⁴⁷ A.C. Ruggeri,²² C. Ruggles,¹³ A. Rychter,⁶¹ K. Sakashita,^{15,†} F. Sánchez,¹² G. Santucci,⁶⁶ C.M. Schloesser,¹⁰ K. Scholberg,^{8,‡} M. Scott,²⁰ Y. Seiya,^{40,††} T. Sekiguchi,^{15,†} H. Sekiya,^{53,27,‡} A. Shaikhiev,²⁵ A. Shaykina,²⁵ M. Shiozawa,^{53,27} W. Shorrocks,²⁰ A. Shvartsman,²⁵ K. Skwarczynski,³⁷ M. Smy,⁴ J.T. Sobczyk,⁶⁴ H. Sobel,^{4,27} F.J.P. Soler,¹³ Y. Sonoda,⁵³ S. Suvorov,^{25,5} A. Suzuki,³⁰ S.Y. Suzuki,^{15,†} Y. Suzuki,²⁷ A.A. Sztuc,²⁰ M. Tada,^{15,†} M. Tajima,³¹ A. Takeda,⁵³ Y. Takeuchi,^{30,27} H.K. Tanaka,^{53,‡} Y. Tanihara,⁶⁵ M. Tani,³¹ N. Teshima,⁴⁰ L.F. Thompson,⁴⁸ W. Toki,⁷ C. Touramanis,³³ T. Towstego,⁵⁸ K.M. Tsui,³³ T. Tsukamoto,^{15,†} M. Tzanov,³⁴ Y. Uchida,²⁰ M. Vagins,^{27,4} S. Valder,⁶² D. Vargas,¹⁷ G. Vasseur,⁵ W.G.S. Vinning,⁶² T. Vladislavjevic,⁵¹ T. Wachala,¹⁴ J. Walker,⁶³ J.G. Walsh,³² Y. Wang,³⁸ D. Wark,^{51,41} M.O. Wascko,²⁰ A. Weber,^{51,41} R. Wendell,^{31,‡} M.J. Wilking,³⁸ C. Wilkinson,² J.R. Wilson,²⁹ K. Wood,³⁸ C. Wret,⁴⁵ K. Yamamoto,^{40,††} C. Yanagisawa,^{38,‡‡} G. Yang,³⁸ T. Yano,⁵³ K. Yasutome,³¹ N. Yershov,²⁵ M. Yokoyama,^{52,‡} T. Yoshida,⁵⁵ M. Yu,⁶⁶ A. Zalewska,¹⁴ J. Zalipska,³⁷ K. Zaremba,⁶¹ G. Zarnecki,³⁷ M. Ziembicki,⁶¹ M. Zito,⁵⁰ and S. Zsoldos²⁹

(The T2K Collaboration)

¹University Autonoma Madrid, Department of Theoretical Physics, 28049 Madrid, Spain

²University of Bern, Albert Einstein Center for Fundamental Physics, Laboratory for High Energy Physics (LHEP), Bern, Switzerland

³Boston University, Department of Physics, Boston, Massachusetts, U.S.A.

⁴University of California, Irvine, Department of Physics and Astronomy, Irvine, California, U.S.A.

⁵IRFU, CEA, Universit Paris-Saclay, F-91191 Gif-sur-Yvette, France

⁶University of Colorado at Boulder, Department of Physics, Boulder, Colorado, U.S.A.

⁷Colorado State University, Department of Physics, Fort Collins, Colorado, U.S.A.

⁸Duke University, Department of Physics, Durham, North Carolina, U.S.A.

- ⁹*Ecole Polytechnique, IN2P3-CNRS, Laboratoire Leprince-Ringuet, Palaiseau, France*
- ¹⁰*ETH Zurich, Institute for Particle Physics and Astrophysics, Zurich, Switzerland*
- ¹¹*CERN European Organization for Nuclear Research, CH-1211 Genve 23, Switzerland*
- ¹²*University of Geneva, Section de Physique, DPNC, Geneva, Switzerland*
- ¹³*University of Glasgow, School of Physics and Astronomy, Glasgow, United Kingdom*
- ¹⁴*H. Niewodniczanski Institute of Nuclear Physics PAN, Cracow, Poland*
- ¹⁵*High Energy Accelerator Research Organization (KEK), Tsukuba, Ibaraki, Japan*
- ¹⁶*University of Houston, Department of Physics, Houston, Texas, U.S.A.*
- ¹⁷*Institut de Fisica d'Altes Energies (IFAE), The Barcelona Institute of Science and Technology, Campus UAB, Bellaterra (Barcelona) Spain*
- ¹⁸*IFIC (CSIC & University of Valencia), Valencia, Spain*
- ¹⁹*Institute For Interdisciplinary Research in Science and Education (IFIRSE), ICISE, Quy Nhon, Vietnam*
- ²⁰*Imperial College London, Department of Physics, London, United Kingdom*
- ²¹*INFN Sezione di Bari and Università e Politecnico di Bari, Dipartimento Interuniversitario di Fisica, Bari, Italy*
- ²²*INFN Sezione di Napoli and Università di Napoli, Dipartimento di Fisica, Napoli, Italy*
- ²³*INFN Sezione di Padova and Università di Padova, Dipartimento di Fisica, Padova, Italy*
- ²⁴*INFN Sezione di Roma and Università di Roma "La Sapienza", Roma, Italy*
- ²⁵*Institute for Nuclear Research of the Russian Academy of Sciences, Moscow, Russia*
- ²⁶*International Centre of Physics, Institute of Physics (IOP), Vietnam Academy of Science and Technology (VAST), 10 Dao Tan, Ba Dinh, Hanoi, Vietnam*
- ²⁷*Kavli Institute for the Physics and Mathematics of the Universe (WPI), The University of Tokyo Institutes for Advanced Study, University of Tokyo, Kashiwa, Chiba, Japan*
- ²⁸*Keio University, Department of Physics, Kanagawa, Japan*
- ²⁹*King's College London, Department of Physics, Strand, London WC2R 2LS, United Kingdom*
- ³⁰*Kobe University, Kobe, Japan*
- ³¹*Kyoto University, Department of Physics, Kyoto, Japan*
- ³²*Lancaster University, Physics Department, Lancaster, United Kingdom*
- ³³*University of Liverpool, Department of Physics, Liverpool, United Kingdom*
- ³⁴*Louisiana State University, Department of Physics and Astronomy, Baton Rouge, Louisiana, U.S.A.*
- ³⁵*Michigan State University, Department of Physics and Astronomy, East Lansing, Michigan, U.S.A.*
- ³⁶*Miyagi University of Education, Department of Physics, Sendai, Japan*
- ³⁷*National Centre for Nuclear Research, Warsaw, Poland*
- ³⁸*State University of New York at Stony Brook, Department of Physics and Astronomy, Stony Brook, New York, U.S.A.*
- ³⁹*Okayama University, Department of Physics, Okayama, Japan*
- ⁴⁰*Osaka City University, Department of Physics, Osaka, Japan*
- ⁴¹*Oxford University, Department of Physics, Oxford, United Kingdom*
- ⁴²*University of Pennsylvania, Department of Physics and Astronomy, Philadelphia, PA, 19104, USA.*
- ⁴³*University of Pittsburgh, Department of Physics and Astronomy, Pittsburgh, Pennsylvania, U.S.A.*
- ⁴⁴*Queen Mary University of London, School of Physics and Astronomy, London, United Kingdom*
- ⁴⁵*University of Rochester, Department of Physics and Astronomy, Rochester, New York, U.S.A.*
- ⁴⁶*Royal Holloway University of London, Department of Physics, Egham, Surrey, United Kingdom*
- ⁴⁷*RWTH Aachen University, III. Physikalisches Institut, Aachen, Germany*
- ⁴⁸*University of Sheffield, Department of Physics and Astronomy, Sheffield, United Kingdom*
- ⁴⁹*University of Silesia, Institute of Physics, Katowice, Poland*
- ⁵⁰*Sorbonne Université, Université Paris Diderot, CNRS/IN2P3, Laboratoire de Physique Nucléaire et de Hautes Energies (LPNHE), Paris, France*
- ⁵¹*STFC, Rutherford Appleton Laboratory, Harwell Oxford, and Daresbury Laboratory, Warrington, United Kingdom*
- ⁵²*University of Tokyo, Department of Physics, Tokyo, Japan*
- ⁵³*University of Tokyo, Institute for Cosmic Ray Research, Kamioka Observatory, Kamioka, Japan*
- ⁵⁴*University of Tokyo, Institute for Cosmic Ray Research, Research Center for Cosmic Neutrinos, Kashiwa, Japan*
- ⁵⁵*Tokyo Institute of Technology, Department of Physics, Tokyo, Japan*
- ⁵⁶*Tokyo Metropolitan University, Department of Physics, Tokyo, Japan*
- ⁵⁷*Tokyo University of Science, Faculty of Science and Technology, Department of Physics, Noda, Chiba, Japan*
- ⁵⁸*University of Toronto, Department of Physics, Toronto, Ontario, Canada*
- ⁵⁹*TRIUMF, Vancouver, British Columbia, Canada*
- ⁶⁰*University of Warsaw, Faculty of Physics, Warsaw, Poland*
- ⁶¹*Warsaw University of Technology, Institute of Radioelectronics and Multimedia Technology, Warsaw, Poland*
- ⁶²*University of Warwick, Department of Physics, Coventry, United Kingdom*
- ⁶³*University of Winnipeg, Department of Physics, Winnipeg, Manitoba, Canada*
- ⁶⁴*Wroclaw University, Faculty of Physics and Astronomy, Wroclaw, Poland*
- ⁶⁵*Yokohama National University, Department of Physics, Yokohama, Japan*
- ⁶⁶*York University, Department of Physics and Astronomy, Toronto, Ontario, Canada*

(Dated: August 19, 2020)

We report measurements by the T2K experiment of the parameters θ_{23} and Δm_{32}^2 which govern the disappearance of muon neutrinos and antineutrinos in the three-flavor PMNS neutrino oscillation model at T2K’s neutrino energy and propagation distance. Utilizing the ability of the experiment to run with either a mainly neutrino or a mainly antineutrino beam, muon-like events from each beam mode are used to measure these parameters separately for neutrino and antineutrino oscillations. Data taken from 1.49×10^{21} protons on target (POT) in neutrino mode and 1.64×10^{21} POT in antineutrino mode are used. Assuming the normal neutrino mass ordering the best-fit values obtained by T2K were $\sin^2(\theta_{23}) = 0.51_{-0.07}^{+0.06}$ ($0.43_{-0.05}^{+0.21}$) and $\Delta m_{32}^2 = 2.47_{-0.09}^{+0.08}$ ($2.50_{-0.13}^{+0.18}$) $\times 10^{-3} \text{eV}^2/c^4$ for neutrinos (antineutrinos). No significant differences between the values of the parameters describing the disappearance of muon neutrinos and antineutrinos were observed. An analysis using an effective two-flavor neutrino oscillation model where the sine of the mixing angle is allowed to take non-physical values larger than 1 is also performed to check the consistency of our data with the three-flavor model. Our data were found to be consistent with a physical value for the mixing angle.

INTRODUCTION

We present an update of T2K’s muon neutrino and antineutrino disappearance measurement from [1] with a larger statistical sample and significant analysis improvements. Data taken up until the end of 2018 are used. This is a beam exposure of 1.49×10^{21} (1.64×10^{21}) protons on target in neutrino (antineutrino) mode; an increase by a factor of 2.0 (2.2) over the previous result. The same data were also used for the result reported in [2]. However, the result reported here focuses on events containing muon neutrino and antineutrino candidates. These events are used to search for potential differences between neutrinos and antineutrinos and also to test consistency with the PMNS oscillation model, by adding additional degrees of freedom to the formulae for calculating the oscillation probability in the present analysis. These additional degrees of freedom are more straightforward to implement and interpret when studying muon-like events only.

The mixing of the three standard flavors of neutrinos without the presence of sterile neutrinos or non-standard interactions is usually described using the PMNS formalism [3, 4]. In this formalism the vacuum oscillation probability is determined by 6 parameters: three angles (θ_{12} , θ_{13} and θ_{23}), two mass squared splittings (Δm_{21}^2 and Δm_{32}^2 , where $\Delta m_{ij}^2 = m_i^2 - m_j^2$) and a complex phase (δ_{CP}). An open question in neutrino oscillations is whether the smaller of the two mass splittings is between the two lightest states or the two heaviest states. These two cases are called the normal and inverted ordering, respectively. Muon neutrino disappearance is not sensitive to the neutrino mass ordering, so all results here assume the normal mass ordering where the third neutrino state is heavier than the two close together states.

In this model, which assumes CPT conservation, muon neutrinos and antineutrinos have identical survival probabilities for vacuum oscillations. At T2K’s beam energy and baseline, the effect of the neutrinos propagating through matter on the muon neutrino survival probability is very small. Therefore, if the oscillation probabilities for neutrinos and antineutrinos differ by significantly more than expected, this could be interpreted as possible

CPT violation and/or non-standard interactions [5, 6].

In the three-flavor analysis presented here, the oscillation probabilities for muon neutrinos and antineutrinos are calculated using the standard PMNS formalism; however we use independent parameters to describe $\bar{\nu}_\mu$ and ν_μ oscillations, i.e. $\bar{\theta}_{23} \neq \theta_{23}$ and $\overline{\Delta m}_{32}^2 \neq \Delta m_{32}^2$, where the barred parameters affect the antineutrino probabilities. The other four oscillation parameters are assumed to be the same for neutrinos and antineutrinos since this data set does not constrain them.

Whilst it does allow the neutrino and antineutrino PMNS parameters to take different values, this three-flavor analysis does not allow the oscillation probabilities to take values not allowed by the PMNS formalism. In order to test consistency with the PMNS formalism we also present an analysis assuming ‘two-flavor’ only oscillations (i.e. $\theta_{13} = 0$), in which $\sin^2(2\theta)$ is allowed to take values exceeding 1, where θ is the effective neutrino mixing angle in a two-flavor oscillation framework. This extension allows the oscillation probability to exceed the maximum possible in the PMNS formalism. ‘Two-flavor’ only oscillations are used for computational simplicity, as the muon neutrino survival probability is not significantly affected by θ_{13} . This two-flavor approximation gives oscillation probabilities that agree to better than 0.5% with the full three-flavor calculation across T2K’s neutrino energy range at the best-fit parameter values from T2K’s joint muon and electron-like event analysis [2].

EXPERIMENTAL APPARATUS

The T2K experiment [7] searches for neutrino oscillations in a long-baseline (295 km) neutrino beam sent from the Japan Proton Accelerator Research Complex (JPARC) in Tokai, Japan to the Super-Kamiokande (SK) detector. SK [8, 9], is situated 2.5° off the axis of the beam. SK’s position off-axis means that it is exposed to a relatively narrow energy width neutrino flux, peaked around the oscillation maximum 0.6 GeV, with a reduced background rate from higher-energy neutrino interactions and reduced contamination from ν_e and $\bar{\nu}_e$ in

the unoscillated beam.

The neutrino beam generation starts with 30 GeV primary protons, produced by J-PARC. These protons strike a graphite target, producing hadrons — primarily pions and kaons. These hadrons are charge-selected and focused by three magnetic horns [10], and decay in a 96 m long decay volume producing neutrinos. These neutrinos are predominantly muon neutrinos. By changing the polarity of the magnetic horn system it is possible to select positively or negatively charged hadrons and thereby create a beam dominated by neutrinos or antineutrinos, respectively. The neutrino energy spectrum varies as a function of the angle to the beam axis.

A set of near detectors measures the unoscillated neutrino beam 280 m downstream of the interaction target.

The on-axis near detector, INGRID [11], is composed of an array of iron/scintillator sandwiches, comprising 7 vertical and 7 horizontal modules arranged in a cross pattern centered on the beam axis. INGRID measures the neutrino beam direction, stability and profile [12].

The off-axis near detector, ND280, is composed of a water-scintillator detector optimized to identify neutral pions (PØD) [13], a tracker consisting of three time projection chambers (TPCs) [14] and two fine-grained detectors (FGD1 and FGD2) [15], and an electromagnetic calorimeter (ECal) [16], which surrounds the PØD and the tracker. The whole off-axis detector is placed in a 0.2 T magnetic field provided by the magnet of the former UA1 and NOMAD experiments at CERN. A side muon range detector (SMRD) [17] is located inside the magnet yokes. The combination of the magnetic field with the tracking TPC detectors allows the momentum and charge of particles to be determined. ND280 characterises the neutrino beam and its interactions before oscillations. The primary contribution of ND280 to the analyses presented here is to constrain the ν_μ and $\bar{\nu}_\mu$ flux, the intrinsic ν_e and $\bar{\nu}_e$ contamination of the beam and the interaction cross sections of different neutrino reactions.

The far detector, SK [8, 9] is a 50 kt water Cherenkov detector, 39 m in diameter and 42 m tall, equipped with 11,129 inward facing 20-inch photomultiplier tubes (PMTs) that image neutrino interactions in the pure water of the inner detector. Additionally, SK has 1,885 outward-facing 8-inch PMTs which instrument the outer detector, mainly used to veto events whose interaction vertex is outside the inner detector. Events at SK are timed using a clock synchronized with the T2K beam line using a GPS system providing synchronisation at the level of O(50 ns) [7].

ANALYSIS DESCRIPTION

The analysis presented here follows the same strategy as that in T2K’s PMNS three-flavor joint fit to muon

disappearance and electron appearance data where neutrinos and antineutrinos are described using the same parameters [2]. A model is constructed that allows predictions to be made of the spectra that will be observed at the near and far detectors. This model uses simulations of the neutrino flux, interaction cross sections and detector response and has variable parameters to account for both systematic and oscillation parameters. First a fit of this model is performed to the near-detector data to constrain the neutrino flux and interaction cross-section uncertainties. The results of this fit are then propagated to the far detector as a multivariate normal distribution described by a covariance matrix and the best-fit values for each systematic parameter. A fit is then performed to the far-detector data to constrain the oscillation parameters. This section describes each part of the analysis focussing on changes from the analysis reported in [1]. Where not stated the same procedure as in [2] is used. Particularly, the beam flux prediction, neutrino interaction modeling, systematic uncertainties and near detector event selection are unchanged and the far-detector event selection used in this result is a subset of that in [2].

Beam flux prediction

The T2K neutrino flux and energy spectrum prediction is discussed extensively in [18]. A FLUKA2011 [19, 20] and GEANT3 [21] based simulation models the physical processes involved in the production of the neutrino beam, from the interaction of primary beam protons in the T2K target, to the decay of hadrons and muons that produce neutrinos.

The modeling of hadronic interactions is constrained by thin target hadron production data, including charged pion and kaon measurements, from the NA61/SHINE experiment at CERN [22–26]. Before any constraint by the ND280 analysis, the systematic uncertainties on the expected number of muon-like events after oscillations at SK due to the beam flux model are 8% and 7.3% for the muon neutrino and antineutrino beams, respectively. In the future this uncertainty will be significantly reduced by including recent hadroproduction measurements by NA61/SHINE using a T2K replica target [27, 28].

Neutrino interaction models

While the neutrino and antineutrino oscillation probabilities are expected to be symmetric, their interaction probabilities with matter are not. For example, the interaction cross section for a charged-current quasielastic (CCQE) interaction on oxygen, which is the most common interaction in water at T2K’s \sim GeV beam energy, is approximately 4 times higher for neutrinos than antineutrinos.

We model neutrino interactions using the NEUT neutrino interaction generator [29]. The neutrino interaction cross-section model and uncertainties used in this result are the same as in [2]. This model is significantly improved compared to the previous version of this analysis [1]. The treatment of multinucleon so-called 2p2h interactions [30, 31] has been updated, with new uncertainties added to the model to account for different rates of this interaction for neutrinos and antineutrinos and different rates for carbon and oxygen targets. We also allow the shape of the interaction cross section for 2p2h in energy-momentum transfer space to vary between that expected for a fully Δ -exchange type interaction and that expected for a fully non- Δ -exchange like interaction.

An uncertainty on the shielding of nucleons by the nucleus in CCQE interactions, modeled using the Nieves random phase approximation (RPA) method, has been added to the analysis [32–35]. Furthermore, the analysis now accounts for mismodeling that could take place due to choosing an incorrect value for the nucleon removal energy in the CCQE process. Finally, we have performed a fit to external data [36, 37] to better constrain our uncertainties describing the resonant single-pion production process.

Near detector event selection

We use the near detector to tune the central values of and constrain the uncertainties on our models of the neutrino flux and neutrino interaction cross section. Particularly, the near-detector analysis reduces our overall uncertainty on the number of events predicted at SK by introducing strong anticorrelations between parameters characterising the systematic uncertainties on the neutrino flux and the neutrino interaction rates.

We define a total of 14 samples of near-detector events, each designed to give us the necessary sensitivity to constrain a particular part of our flux or cross-section model. All selected events must have a reconstructed charged muon present, as we are targeting charged-current (CC) neutrino interactions. We also require that the muon is the highest momentum track in the event. In neutrino beam mode, the muon is required to be negatively charged as this is the expected charge for muons originating from a CC neutrino interaction. The neutrino mode event samples are separated down by the number of pions reconstructed: 0, 1 positively charged pion and any other number of pions. These samples are enriched in events from CCQE, CC single pion and CC deep inelastic scattering interactions, respectively.

In antineutrino beam mode there is one set of samples for positively charged muons and one set for negatively charged muons. This allows a separate constraint of the neutrino and antineutrino composition of the beam. This constraint is particularly important in antineutrino mode

due to the larger interaction cross section for neutrinos than antineutrinos. The antineutrino samples are separated based on the number of reconstructed tracks that are matched between the TPC and FGD: 1 or more than 1. These samples are enriched in events from CCQE and CC non-QE interactions, respectively.

Both neutrino and antineutrino mode samples are further separated according to whether their vertices are reconstructed in FGD1 (CH target) or in FGD2 (42% water, 58% CH by mass).

As in [2], the near-detector data set for antineutrino mode is 1.38 times larger than in [1], while the neutrino mode data set is the same size.

Far detector event selection

The analyses presented here target muon-like events. One feature of SK is that it is not able to distinguish neutrinos from antineutrinos at an event by event level since the charge of the outgoing leptons cannot be reconstructed. Hence, we gain our ability to separately measure neutrino and antineutrino oscillations by forming two samples of muon-like events, one collected when the beam is run in neutrino mode, and one collected when the beam is run in antineutrino mode.

The vertex position, momentum reconstruction, and particle identification (PID) in SK is performed by observing the Cherenkov radiation produced by charged particles traversing the detector. This radiation forms ring patterns that are recorded by the PMTs. Particle identification is possible because muons/antimuons produced by $\nu_\mu/\bar{\nu}_\mu$ CC interactions proceed with little scattering through the water due to their large mass and hence produce a clear ring pattern. In contrast, electrons from ν_e and positrons from $\bar{\nu}_e$ CC interactions produce electromagnetic showers resulting in Cherenkov rings with diffuse edges. In addition to the shape of the Cherenkov ring, the opening angle of the ring also helps to distinguish between electrons and muons. The samples used in the analyses here require exactly one muon-like Cherenkov ring and no other rings to be reconstructed. The samples are therefore referred to as $1R\mu$.

T2K's reconstruction algorithm uses a maximum-likelihood based approach taking in the number of photons observed by and the timing information from each of the PMTs in SK [38]. Compared to the previous algorithm that was used in [1], this approach allows an increase of the fiducial volume by approximately 20% due to better signal-background discrimination.

Both $1R\mu$ samples use the same selection criteria. Events must be fully contained within the far detector, with no activity in the SK outer detector. Event vertices are required to be a certain distance from the tank wall, and the reconstructed momentum of the muons has to be greater than 200 MeV. Table I shows the number of

Sample	Prediction	Data
ν -mode 1R μ	272.34	243
$\bar{\nu}$ -mode 1R μ	139.47	140

TABLE I. Number of events predicted using the best-fit oscillation parameter values from a previous T2K oscillation analysis [36], and the number of data events collected for both 1R μ samples.

events for both 1R μ samples predicted using the best-fit values of the oscillation parameters from a previous T2K analysis [36], and the number of events actually selected from the data.

Systematic uncertainties and oscillation analysis

As described above, our model includes systematic uncertainties from the neutrino flux prediction, the neutrino interaction cross-section model and detector effects. We constrain several of these uncertainties by fitting our model to ND280 near-detector data. The near-detector samples are binned in muon momentum and angle. This ND280 constrained model is then used as the prior in the fits to the far-detector data, where the SK muon-like samples are binned in the neutrino energy reconstructed using lepton momentum and angle assuming a CCQE interaction. Table II shows the total systematic error in each 1R μ sample and a breakdown of the contributions from each uncertainty source. As discussed above the near-detector fit introduces large anticorrelations between the parameters modeling the flux and cross-section uncertainties, so Table II also lists the overall contribution to the uncertainty from the combination of flux and cross-section uncertainties.

The near-detector analysis reduces the systematic error on the expected number of events in the neutrino (antineutrino) mode 1R μ sample from 15 (13)% down to 5.5 (4.4)%.

In the three-flavor analysis, the oscillation probabilities for neutrino and antineutrino events are calculated using the full three-flavor oscillation formulae [39], including matter effects, with a crust density of $\rho = 2.6 \text{ g/cm}^3$ [40]. As described in the introduction, for neutrino events we allow the values of θ_{23} and Δm_{32}^2 used in the neutrino oscillation probability calculation to vary independently from those used for the antineutrino oscillation probability, in order to search for potential differences between neutrino and antineutrino oscillations.

In the two-flavor analysis, we use a modified version of the canonical two-flavor oscillation formula [41], in which the disappearance probability for muon (anti-) neutrinos is given by:

$$P_{\nu_\mu \rightarrow \nu_\mu} (P_{\bar{\nu}_\mu \rightarrow \bar{\nu}_\mu}) \approx 1 - \alpha(\bar{\alpha}) \sin^2 \left(1.267 \frac{\Delta m^2 [\text{eV}^2] L [\text{km}]}{E [\text{GeV}]} \right)$$

Error source	1R μ ν -mode	1R μ $\bar{\nu}$ -mode
Flux (constr. by ND280)	4.3%	4.1%
Xsec (constr. by ND280)	4.7%	4.0%
Xsec (all)	5.6%	4.4%
Flux + Xsec (constr. by ND280)	3.3%	2.9%
Flux + Xsec (all)	5.4%	3.2%
SK detector effects+FSI+SI	3.3%	2.9%
Total	5.5%	4.4%

TABLE II. Systematic uncertainty on the number of events in each of the 1R μ samples broken down by uncertainty source. Neutrino cross-section parameter uncertainties (denoted ‘xsec’) are further broken down by whether they are constrained by our fit to ND280 data or not. Uncertainties due to final state interactions (FSI) and secondary interactions (SI) are incorporated in the analysis by adding them to the SK detector effect uncertainty, so the impact of these uncertainties is listed together.

where the variable α plays the role of the well-known effective two flavor mixing angle, $\sin^2 2\theta$. However, α differs from $\sin^2 2\theta$ in that it is allowed to take values larger than 1. The effective two-flavor Δm^2 used here can be obtained from the three-flavor oscillation parameters using the following equation:

$$\Delta m^2 = \Delta m_{32}^2 + \sin^2 \theta_{12} \Delta m_{21}^2 + \cos \delta_{CP} \sin \theta_{13} \sin 2\theta_{12} \tan \theta_{23} \Delta m_{21}^2.$$

As in the three-flavor analysis we allow the oscillation parameters affecting neutrinos and antineutrinos to vary independently, with α and Δm^2 affecting neutrinos, and $\bar{\alpha}$ and Δm^2 affecting antineutrinos.

One feature of this effective treatment is that when $\alpha > 1.0$, the survival probability of muon (anti-)neutrinos is negative at some points in $(\Delta m^2, E_\nu)$ parameter space. When weighting our Monte Carlo to produce predicted spectra for these points of parameter space we therefore obtain negative oscillation probability weights for some events. We allow these negative event weights. However, we do not allow the total predicted number of events in any bin of our event samples to be negative, setting them instead to 10^{-6} where this occurs.

For both the two-flavor and three-flavor analyses, a joint maximum-likelihood fit to both 1R μ samples is performed. The likelihood used is a marginal likelihood where all parameters except the parameters of interest are marginalized over.

The marginalization consists of integrating the likelihood over the nuisance parameters, weighted by a prior taken from the uncertainty model after the fit to ND280 data. The priors for the neutrino oscillation parameters used in the three-flavor analysis are shown in Table III, while θ_{12} and Δm_{12}^2 are fixed at their values from [42], due to their negligible effect on the muon neutrino disappearance probability. The prior on θ_{13} is taken from

[42].

Numerically the marginalization is carried out by randomly throwing a large number of vectors of these nuisance parameters from their prior distributions and calculating the average likelihood across the different throws.

Parameter	Prior
$\sin^2 2\theta_{13}$	Gaussian ($\mu = 0.0830$, $\sigma = 0.0032$)
δ_{CP}	Uniform $[-\pi, \pi]$
$\sin^2 \theta_{23}$	Uniform $[0, 1]$
Δm_{32}^2	Uniform $[2.2 \times 10^{-3}, 3.0 \times 10^{-3}] \text{ eV}^2/c^4$

TABLE III. Prior distributions marginalised over for oscillation parameters in the three-flavor analysis.

We build frequentist confidence intervals assuming the critical values for $\Delta\chi^2$ from a standard χ^2 distribution. $\Delta\chi^2$ is defined as the difference between the minimum χ^2 and the value for a given point in parameter space.

RESULTS AND DISCUSSION

The reconstructed energy spectra of the ν_μ and $\bar{\nu}_\mu$ events observed during neutrino and antineutrino running modes are shown in Fig. 1. All fits discussed below are to both $1R\mu$ samples unless stated otherwise.

Three-flavor analysis

Assuming normal ordering, the best-fit values obtained for the parameters describing neutrino oscillations are $\sin^2 \theta_{23} = 0.51^{+0.06}_{-0.07}$ and $\Delta m_{32}^2 = 2.47^{+0.08}_{-0.09} \times 10^{-3} \text{ eV}^2/c^4$, and those describing antineutrino oscillations are $\sin^2 \bar{\theta}_{23} = 0.43^{+0.21}_{-0.05}$ and $\overline{\Delta m_{32}^2} = 2.50^{+0.18}_{-0.13} \times 10^{-3} \text{ eV}^2/c^4$. The best-fit value and uncertainty on $\overline{\Delta m_{32}^2}$ obtained assuming normal ordering are equivalent to those that would be obtained on $\overline{\Delta m_{31}^2}$ assuming inverted ordering.

In Fig. 2, we show the confidence intervals obtained on the oscillation parameters applying to neutrinos overlaid on those for the parameters applying to antineutrinos. As the parameters for neutrinos and antineutrinos show no significant incompatibility, this analysis provides no indication of new physics. For comparison we also show the confidence interval obtained on Δm_{32}^2 and $\sin^2 \theta_{23}$ from the fit to electron-like and muon-like data in [2]. One can see by comparing the muon-like only and the joint muon-like and electron-like fits that T2K's sensitivity to whether $\sin^2 \theta_{23}$ is above or below 0.5 is mostly driven by the electron-like samples as expected, as the muon disappearance probability depends at leading order on the sine squared of twice the mixing angle.

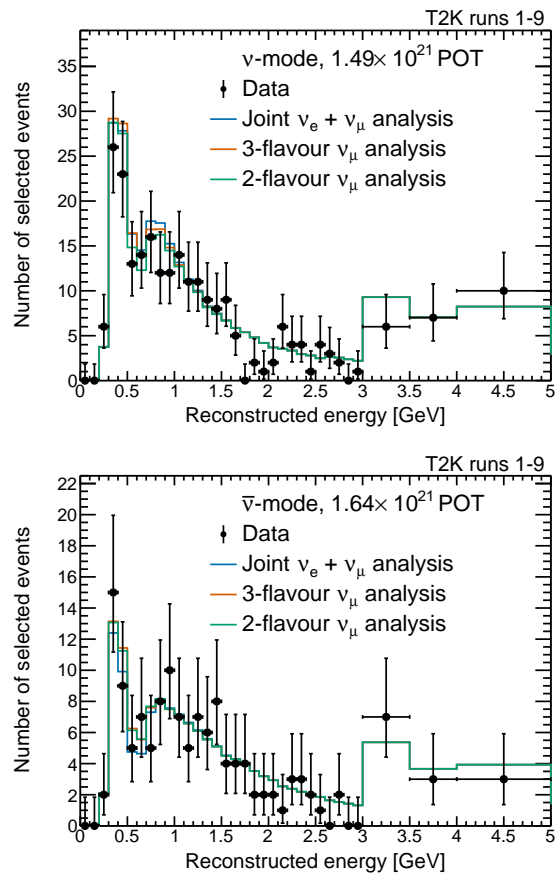


FIG. 1. Reconstructed energy spectra are shown for the $1R\mu$ samples. The top panel shows the neutrino mode sample, while the bottom panel shows the antineutrino mode sample. The black points show the number of observed data events, while the lines show the predicted number of events from simulation under several oscillation hypotheses. ‘Joint ν_e/ν_μ analysis’ is the prediction for the best-fit value from a joint fit to electron-like and muon-like data with standard PMNS oscillations from [2]. ‘3-flavor ν_μ analysis’ is the prediction for the best-fit value in the three-flavor fit reported here to the muon-like data. ‘2-flavor ν_μ analysis’ is the prediction for the best-fit value in the two flavor fit reported here to the muon-like data. The uncertainty range shown around the data points is chosen to include all predicted event rates for which the measured number of data events is inside the 68% confidence interval of a Poisson distribution centred at that prediction.

Two-flavor consistency check analysis

The best-fit values obtained on the effective two-flavor oscillation parameters are $\Delta m^2 = 2.49^{+0.08}_{-0.08} \times 10^{-3} \text{ eV}^2/c^4$, $\alpha = 1.008^{+0.017}_{-0.016}$, $\overline{\Delta m^2} = 2.51^{+0.15}_{-0.14} \times 10^{-3} \text{ eV}^2/c^4$, $\bar{\alpha} = 0.976^{+0.029}_{-0.029}$. Fig. 3 shows the 68% and 90% confidence intervals for $(\Delta m^2, \alpha)$ and $(\overline{\Delta m^2}, \bar{\alpha})$. Both the 1σ confidence intervals include values of $\alpha(\bar{\alpha}) \leq 1.0$, indicating no significant disagreement between data and standard physical PMNS neutrino oscillations. We also see good

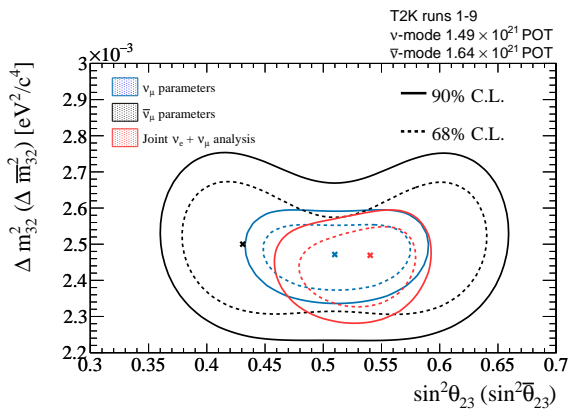


FIG. 2. 68% and 90% confidence intervals on $\sin^2 \theta_{23}$ and Δm_{32}^2 are shown in blue and on $\sin^2 \bar{\theta}_{23}$ and $\Delta \bar{m}_{32}^2$ are shown in black. These intervals are obtained from a fit to the neutrino and antineutrino mode $1R\mu$ samples using the three-flavor analysis described here. Normal ordering is assumed. Equivalent intervals on $\sin^2 \theta_{23}$ and Δm_{32}^2 are shown in red from a joint fit to muon-like and electron-like T2K data described in [2].

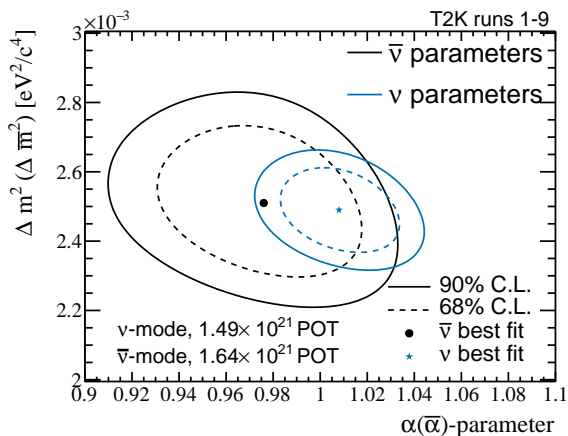


FIG. 3. 68% and 90% confidence intervals on the two-flavor analysis parameters affecting neutrinos ($\Delta m^2, \alpha$), and antineutrinos ($\Delta \bar{m}^2, \bar{\alpha}$).

compatibility between the parameters affecting neutrinos and antineutrinos.

Conclusions

We have presented separate measurements of the oscillation parameters governing muon neutrino disappearance and muon antineutrino disappearance in long-baseline neutrino experiments. This analysis uses a significantly larger data sample and a much improved model of systematic uncertainties than those used in T2K's previous measurement of these parameters in [1]. We also present a consistency check between our data and the

PMNS oscillation framework, where $\sin^2(2\theta)$ is allowed to take values larger than 1. In all analyses we find the neutrino and antineutrino oscillation parameters are compatible with each other, and that our data are compatible with the PMNS oscillation framework. It should be noted that the results from these fits improve upon the sensitivity of previous results of separate fits to muon neutrino and antineutrino disappearance by the MINOS collaboration [43] and that there is no significant disagreement with these previous results (both show values of Δm_{32}^2 around $2.5 \times 10^{-3} \text{eV}^2/c^4$ and θ_{23} consistent with maximal mixing).

We thank the J-PARC staff for superb accelerator performance. We thank the CERN NA61/SHINE Collaboration for providing valuable particle production data. We acknowledge the support of MEXT, Japan; NSERC (grant number SAPPJ-2014-00031), the NRC and CFI, Canada; the CEA and CNRS/IN2P3, France; the DFG, Germany; the INFN, Italy; the National Science Centre and Ministry of Science and Higher Education, Poland; the RSF (grant number 19-12-00325) and the Ministry of Science and Higher Education, Russia; MINECO and ERDF funds, Spain; the SNSF and SERI, Switzerland; the STFC, UK; and the DOE, USA. We also thank CERN for the UA1/NOMAD magnet, DESY for the HERA-B magnet mover system, NII for SINET4, the WestGrid and SciNet consortia in Compute Canada, and GridPP in the United Kingdom. In addition, participation of individual researchers and institutions has been further supported by funds from the ERC (FP7), la Caixa Foundation (ID 100010434, fellowship code LCF/BQ/IN17/11620050), the European Unions Horizon 2020 Research and Innovation Programme under the Marie Skłodowska-Curie grant agreement numbers 713673 and 754496, and H2020 grant numbers RISE-GA822070-JENNIFER2 2020 and RISE-GA872549-SK2HK; the JSPS, Japan; the Royal Society, UK; French ANR grant number ANR-19-CE31-0001; and the DOE Early Career programme, USA.

* also at INFN-Laboratori Nazionali di Legnaro

† also at J-PARC, Tokai, Japan

‡ affiliated member at Kavli IPMU (WPI), the University of Tokyo, Japan

§ also at National Research Nuclear University "MEPhI" and Moscow Institute of Physics and Technology, Moscow, Russia

¶ also at the Graduate University of Science and Technology, Vietnam Academy of Science and Technology

** also at JINR, Dubna, Russia

†† also at Nambu Yoichiro Institute of Theoretical and Experimental Physics (NITEP)

‡‡ also at BMCC/CUNY, Science Department, New York, New York, U.S.A.

- [1] K. Abe *et al.*, “Updated T2K measurements of muon neutrino and antineutrino disappearance using 1.5×10^{21} protons on target,” *Phys. Rev.*, vol. D96, p. 011102, 2017.
- [2] K. Abe *et al.*, “Constraint on the Matter-Antimatter Symmetry-Violating Phase in Neutrino Oscillations,” *Nature*, vol. 580, no. 7803, pp. 339–344, 2020.
- [3] Z. Maki, M. Nakagawa, and S. Sakata, “Remarks on the unified model of elementary particles,” *Prog. Theor. Phys.*, vol. 28, pp. 870–880, 1962.
- [4] B. Pontecorvo, “Neutrino Experiments and the Problem of Conservation of Leptonic Charge,” *Sov. Phys. JETP*, vol. 26, pp. 984–988, 1968. [Zh. Eksp. Teor. Fiz. 53,1717(1967)].
- [5] V. A. Kostelecký and M. Mewes, “Neutrinos with Lorentz-violating operators of arbitrary dimension,” *Phys. Rev. D*, vol. 85, p. 096005, May 2012.
- [6] O. G. Miranda and H. Nunokawa, “Non standard neutrino interactions: current status and future prospects,” *New Journal of Physics*, vol. 17, p. 095002, sep 2015.
- [7] K. Abe *et al.*, “The T2K Experiment,” *Nucl. Instrum. Meth.*, vol. A659, pp. 106–135, 2011.
- [8] Y. Fukuda *et al.*, “The Super-Kamiokande detector,” *Nucl. Instrum. Meth.*, vol. A501, pp. 418–462, 2003.
- [9] K. Abe *et al.*, “Calibration of the Super-Kamiokande Detector,” *Nucl. Instrum. Meth.*, vol. A737, pp. 253–272, 2014.
- [10] T. Sekiguchi *et al.*, “Development and operational experience of magnetic horn system for T2K experiment,” *Nucl. Instrum. Meth.*, vol. A789, pp. 57–80, 2015.
- [11] M. Otani *et al.*, “Design and construction of INGRID neutrino beam monitor for T2K neutrino experiment,” *Nucl. Instrum. Meth.*, vol. A623, pp. 368–370, 2010.
- [12] K. Suzuki *et al.*, “Measurement of the muon beam direction and muon flux for the T2K neutrino experiment,” *PTEP*, vol. 2015, p. 053C01, 2014.
- [13] S. Assylbekov *et al.*, “The T2K ND280 Off-Axis Pi-Zero Detector,” *Nucl. Instrum. Meth.*, vol. A686, pp. 48–63, 2012.
- [14] N. Abgrall *et al.*, “Time projection chambers for the t2k near detectors,” *Nucl. Instrum. Meth.*, vol. 637, pp. 25–46, may 2011.
- [15] P.-A. Amaudruz *et al.*, “The t2k fine-grained detectors,” *Nucl. Instrum. Meth.*, vol. 696, pp. 1–31, dec 2012.
- [16] D. Allan *et al.*, “The Electromagnetic Calorimeter for the T2K Near Detector ND280,” *JINST*, vol. 8, p. P10019, 2013.
- [17] S. Aoki *et al.*, “The T2K Side Muon Range Detector (SMRD),” *Nucl. Instrum. Meth.*, vol. A698, pp. 135–146, 2013.
- [18] K. Abe *et al.*, “T2K neutrino flux prediction,” *Phys. Rev. D*, vol. 87, p. 012001, Jan 2013.
- [19] A. Ferrari, P. R. Sala, A. Fasso, and J. Ranft, “FLUKA: A multi-particle transport code (Program version 2005),” 2005.
- [20] T. Bhlen, F. Cerutti, M. Chin, A. Fass, A. Ferrari, P. Ortega, A. Mairani, P. Sala, G. Smirnov, and V. Vlachoudis, “The fluka code: Developments and challenges for high energy and medical applications,” *Nuclear Data Sheets*, vol. 120, pp. 211 – 214, 2014.
- [21] R. Brun, F. Bruyant, F. Carminati, S. Giani, M. Maire, A. McPherson, G. Patrick, and L. Urban, “GEANT Detector Description and Simulation Tool,” 1994.
- [22] N. Abgrall *et al.*, “Measurements of Cross Sections and Charged Pion Spectra in Proton-Carbon Interactions at 31 GeV/c,” *Phys. Rev.*, vol. C84, p. 034604, 2011.
- [23] N. Abgrall *et al.*, “Measurement of Production Properties of Positively Charged Kaons in Proton-Carbon Interactions at 31 GeV/c,” *Phys. Rev.*, vol. C85, p. 035210, 2012.
- [24] N. Abgrall *et al.*, “Measurements of π^\pm , K^\pm , K_S^0 , Λ and proton production in protoncarbon interactions at 31 GeV/c with the NA61/SHINE spectrometer at the CERN SPS,” *Eur. Phys. J.*, vol. C76, no. 2, p. 84, 2016.
- [25] M. Posiadaa-Zezula, “Recent T2K flux predictions with NA61/SHINE thin graphite target measurements,” *J. Phys. Conf. Ser.*, vol. 888, no. 1, p. 012064, 2017.
- [26] L. Zambelli, “Hadroproduction experiments to constrain accelerator-based neutrino fluxes,” *J. Phys. Conf. Ser.*, vol. 888, no. 1, p. 012021, 2017.
- [27] N. Abgrall *et al.*, “Measurements of π^\pm , K^\pm and proton double differential yields from the surface of the T2K replica target for incoming 31 GeV/c protons with the NA61/SHINE spectrometer at the CERN SPS,” *Eur. Phys. J.*, vol. C79, no. 2, p. 100, 2019.
- [28] N. Abgrall *et al.*, “Measurements of π^\pm differential yields from the surface of the T2K replica target for incoming 31 GeV/c protons with the NA61/SHINE spectrometer at the CERN SPS,” *Eur. Phys. J. C*, vol. 76, no. 11, p. 617, 2016.
- [29] Y. Hayato, “A Neutrino Interaction Simulation Program Library NEUT,” *Acta Physica Polonica B*, vol. 40, p. 2477, Sep 2009.
- [30] J. Nieves, I. R. Simo, and M. J. V. Vacas, “Inclusive charged-current neutrino-nucleus reactions,” *Phys. Rev. C*, vol. 83, p. 045501, Apr 2011.
- [31] R. Gran, J. Nieves, F. Sanchez, and M. J. Vicente Vacas, “Neutrino-nucleus quasi-elastic and 2p2h interactions up to 10 GeV,” *Phys. Rev.*, vol. D88, no. 11, p. 113007, 2013.
- [32] J. Nieves, J. E. Amaro, and M. Valverde, “Inclusive quasielastic charged-current neutrino-nucleus reactions,” *Phys. Rev. C*, vol. 70, p. 055503, Nov 2004.
- [33] J. Nieves, J. E. Amaro, and M. Valverde, “Erratum: Inclusive quasielastic charged-current neutrino-nucleus reactions [phys. rev. c 70, 055503 (2004)],” *Phys. Rev. C*, vol. 72, p. 019902, Jul 2005.
- [34] M. Valverde, J. E. Amaro, and J. Nieves, “Theoretical uncertainties on quasielastic charged-current neutrino-nucleus cross sections,” *Phys. Lett.*, vol. B638, pp. 325–332, 2006.
- [35] R. Gran, “Model uncertainties for Valencia RPA effect for MINERvA,” 2017.
- [36] K. Abe *et al.*, “Search for CP Violation in Neutrino and Antineutrino Oscillations by the T2K Experiment with 2.2×10^{21} Protons on Target,” *Phys. Rev. Lett.*, vol. 121, no. 17, p. 171802, 2018.
- [37] P. Stowell, C. Wret, C. Wilkinson, L. Pickering, S. Cartwright, Y. Hayato, K. Mahn, K. McFarland, J. Sobczyk, R. Terri, L. Thompson, M. Wascko, and Y. Uchida, “NUISANCE: a neutrino cross-section generator tuning and comparison framework,” *Journal of Instrumentation*, vol. 12, pp. P01016–P01016, jan 2017.
- [38] M. Jiang, K. Abe, C. Bronner, Y. Hayato, M. Ikeda, K. Iyogi, J. Kameda, Y. Kato, Y. Kishimoto, L. I. Marti, and et al., “Atmospheric neutrino oscillation analysis with improved event reconstruction in Super-Kamiokande IV,” *Progress of Theoretical and Experimental Physics*, vol. 2019, May 2019.

- [39] V. D. Barger, K. Whisnant, S. Pakvasa, and R. J. N. Phillips, "Matter Effects on Three-Neutrino Oscillations," *Phys. Rev.*, vol. D22, p. 2718, 1980. [,300(1980)].
- [40] K. Hagiwara, N. Okamura, and K. Senda, "The earth matter effects in neutrino oscillation experiments from Tokai to Kamioka and Korea," *JHEP*, vol. 2011, p. 82, Sep 2011.
- [41] H. Nunokawa, S. J. Parke, and R. Zukanovich Funchal, "Another possible way to determine the neutrino mass hierarchy," *Phys. Rev.*, vol. D72, p. 013009, 2005.
- [42] Tanabashi et al., "Review of particle physics," *Phys. Rev. D*, vol. 98, p. 030001, Aug 2018.
- [43] P. Adamson *et al.*, "Combined analysis of ν_μ disappearance and $\nu_\mu \rightarrow \nu_e$ appearance in MINOS using accelerator and atmospheric neutrinos," *Phys. Rev. Lett.*, vol. 112, p. 191801, 2014.